OPEN

Axon Injury and Regeneration in the Adult *Drosophila*

Lorena Soares, Michael Parisi & Nancy M. Bonini

Department of Biology, University of Pennsylvania, Philadelphia, PA, 19104, USA.

Neural regeneration is a fascinating process with profound impact on human health, such that defining biological and genetic pathways is of interest. Here we describe an *in vivo* preparation for neuronal regeneration in the adult *Drosophila*. The nerve along the anterior margin of the wing is comprised of ~225 neurons that send projections into the central neuropil (thorax). Precise ablation can be induced with a pulsed laser to sever the entire axonal tract. The animal can be recovered, and response to injury assessed over time. Upon ablation, there is local loss of axons near the injury site, scar formation, a rapid impact on the cytoskeleton, and stimulation of hemocytes. By 7d, ~50% of animals show nerve regrowth, with axons from the nerve cells extending down towards the injury or re-routing. Inhibition of JNK signaling promotes regrowth through the injury site, enabling regeneration of the axonal tract.

Neural regrowth and regeneration are important health issues, given the high incidence of acute injury and degenerative conditions. In the mammalian central nervous system (CNS), neurons display poor capacity to regrow upon damage, which may reflect a combination of a limited intrinsic regenerative capacity and an un-conducive environment[1–7]. The peripheral nervous system (PNS) has higher regenerative capacity, yet even these often fail to reach their targets. Defining in greater breath and detail pathways that modulate the regenerative capacity of the nervous system could have a profound impact on the development of therapeutics for spinal cord injury and traumatic brain injury.

Experimental models for inducing controlled and reproducible injury have been developed in a number of model organisms[7–13]. Studies in mammals have elucidated basic features of the axonal response to traumatic injury. However, these models are hindered by the poor capacity to regenerate, limited ability to apply large genetic or chemical screens, and need for laborious methods to characterize responses. More recently, *C. elegans* has been used to study axonal regeneration[8,10]. Due to the simplicity of the nematode nervous system, these models are largely limited to identifying factors that impact neuron-intrinsic pathways and individual cells, versus addressing the potential dynamics of more complex systems.

The *Drosophila* nervous system shares features with vertebrates: neurons are bundled into axonal tracts, wrapped in glia and surrounded by circulating hemolymph cells that carry out immune and phagocytic functions. Thus, the fly allows characterization of factors involved in the complex interplay between cell types involved in response to acute neural injury, as well as neural intrinsic players. Several *Drosophila* models have been developed, including a stab wound to the adult fly head using needles to model traumatic brain injury[14], crush models of larval segmental nerves using forceps[15], precise severing of larval nerves by laser ablation to study regeneration[16] among others[17]. Attempts to use the fly for regeneration have largely focused on the larval stage where the capacity for regrowth is robust, although the study of neural regeneration is limited by the short duration of the developmental stage. Molecular mechanisms controlling axon regeneration during development also likely differ from the adult. Indeed a potent modifier of Wallerian degeneration, Wld[s], fails to suppress developmental loss during axon pruning[18], while robustly protecting axons from degeneration in the adult[19,20]. In *Drosophila*, it has been unknown if the adult nervous system can display regenerative capacity, and if so, whether this capacity could be experimentally manipulated.

Here, we describe a reproducible *in vivo Drosophila* model of axon injury by laser ablation of the peripheral nerve of the fly wing. Importantly, this paradigm is in the adult animal and leaves the neural cell bodies intact allowing analysis of the capacity for axonal regrowth. This model will facilitate the identification of factors that impact neural regeneration, providing a new approach for discovery of therapeutics for restoration of nerve function following injury.

Results

An *in vivo* preparation for adult axonal injury. To investigate neural injury in the adult, we explored nerve tracts amenable to laser transection. We first sought ways to mount and immobilize the adult animal in a transient way that would allow for recovery of the fly in order to characterize a response over time. Flies were successfully immobilized by gently mounting them dorsal side down on agarose slides, and maintaining them on ice or light CO_2 until ablation (Supplementary Figure S1). Flies mounted in this manner were readily recovered after the experiment with minimal lethality and no observable defects. Flies could be re-mounted in a similar manner at a later time point following ablation to view the response in the live animal with light microscopy; alternatively, wings could be removed and fixed for detailed analysis by confocal.

Next we examined target nerves in flies that selectively express green fluorescent protein (GFP) in all neurons or in select neurons using the GAL4/UAS system. Whereas most of the fly is protected by a hard thick cuticle, the nerve tracts of the wing were accessible to visualization and precise axotomy (Figure 1, Supplementary Figure S1). The wing is comprised of an epithelial bilayer bearing a stereotypical pattern of veins that conduct hemolymph (Figure 1a, Supplementary Figure 1). Five longitudinal veins (L1-5) run along the anterior-posterior axis. Of these, L1 has mechanosensory and chemosensory nerves, and L3 bears a set of campaniform sensilla and the sensory neurons that innervate them[21,22]. The nerves of the wing margin have their cell bodies spaced along L1 from the point where L1 meets the costal vein, to the tip of the wing where L1 meets L3. Their axons project into the CNS within the thorax (Figure 1a, Supplementary Figure 1). These neurons and their projections were readily visualized and monitored in animals expressing GFP with a neural driver (Figure 1). Highlighting the neurons with GFP using the *appl-GAL4* line, we counted neural cell bodies along the wing margin, using high magnification in multiple wings. The wing margin tract consists of ~225 neural cells, thus the axonal bundle severed is comprised of ~225 axons.

To injure the axons, we used a tunable Micropoint dye laser (Supplementary Figure S1). We established a reproducible ablation site just after the last cluster of L1 neural cell bodies (Figure 1b, arrow), such that the projections of all neurons along the L1 margin were axotomized. The laser power was empirically defined to be the lowest power necessary to successfully cut the axonal bundle; there was no damage to adjacent tissue. Upon ablation, precise and localized severing of the axonal tract was marked by a rapid separation of the two GFP-labeled ends of the nerve fiber (Figure 1c–e, Supplementary Movie 1). The "snapping" of the bundle indicated that it is under tension, and this response was used, along with the GFP signal, as an indication of complete transection of all axons. Severing was distinct from photobleaching of the GFP: by attenuating the laser power and firing continuously for 1 min (Figure 1f), we could bleach the GFP signal through the width of the nerve tract. In this situation, we did not observe a snapping back of the nerve, and the GFP signal readily recovered. This is in sharp contrast to ablations, where GFP recovery was never seen at the injury site. These data indicated that the fly wing was an exceptional preparation for nerve injury where we can approach the L1 nerve, precisely sever the axonal tract, recover the animals and follow progression of the injury response over time.

Characterization of injury-induced axonal response. With this preparation, we performed laser ablation on 6h adult animals, then characterized the response over 14d by examining the GFP pattern. The initial response was a uniform local loss of GFP. The response then resolved to four categories that we refer to as Broad Loss, Local Loss, GFP to Injury, and Misrouting (Figure 2a–d). Any single wing showed only one response: we never saw a mixed biological response

of the wing margin axonal tract. Broad Loss and Local Loss specify categories where axonal degeneration occurred without regrowth or recovery: Broad Loss was extensive GFP loss extending beyond the first neural cell body cluster on the wing margin (Figure 2a, a'); Local Loss were wings in which the GFP pattern reflected loss of signal near the injury site that extended maximally back to the first neural cell body cluster (Figure 2b, b'). The other two categories describe wings in which axonal regrowth occurred based on GFP. GFP to Injury described wings in which the GFP signal from the neurons recovered to the injury site. These wings typically showed thick GFP projections near the injury site, frequently characterized by multiple axonal tracts (Figure 2c). The thick endings often had a fan-like appearance indicative of axonal sprouting. The extent of regrowth from the first neuronal cell bodies within the wing margin to the site of injury was an average of 66 ± 21 μm (mean $\pm$ SD of 6 wings). The final class, Misrouting, described wings with evidence of axonal growth, although the projections misrouted to invade the costal vein (Figure 2d). The distance that the nerve tract regrew to reach the costal from the wing margin was a mean of 51.3 ± 0.9 μm (mean $\pm$ SD, 6 wings); the distance that the nerve projections travelled within the costal was variable, and ranged from 26 to 120 μm (79 ± 31, mean $\pm$ SD, 6 wings). Although we were not able to determine the percentage of axons that regrew, based on thickness of the regrown tract compared to the uninjured tract, the number was considerable (see Figures 2c-c", d-d").

The response to injury was graded over time, showing a differential distribution of classes (Figure 2e). There was a consistent initial response on d1 after axotomy, with 100% of the wings showing local loss near the injury site. By d3, the majority of wings still fell into the category of Local Loss, but a significant number now showed GFP to Injury ($31 \pm 2\%$, mean $\pm$ SD), indicating that axonal growth occurred. By d5, two opposing changes were seen: a fraction of the wings now showed Misrouting ($6 \pm 5\%$, mean $\pm$ SD), whereas a fraction showed more extensive loss of GFP (Broad Loss, $13 \pm 4\%$, mean $\pm$ SD). By d7, the majority of wings showed either GFP to Injury ($42 \pm 7\%$, mean $\pm$ SD) or Misrouting ($21 \pm 7\%$, mean $\pm$ SD), indicating that further axonal growth had taken place. With time, the percentage of wings with Broad Loss increased, such that by 14d, $50 \pm 38\%$ of wings showed Broad Loss with signal loss further toward the distal tip of the wing. We interpreted the transient growth response as evidence of recovery, followed by degeneration of the projections perhaps due to lack of connectivity to targets.

A number of control experiments confirmed that the GFP response was neuronal-injury specific and only seen in wings where axons were severed. First, we performed mock ablations by firing the laser inside the L1 vein next to the axon bundle, but without damaging the tract. Here, we were driving the laser with identical power as for ablation, but in the absence of neural damage. Any effects of the laser (such as heat or penetration through the cuticle) were the same as with neural injury. This control assessed potential effects caused by the laser independent of physical nerve damage. With this treatment, no changes to the GFP pattern were detected, and no other biological changes were detected as detailed for neural injury below: no pigmentation scar formed (Figure 3), no hemocyte response was detected and no effects to the cytoskeleton were observed. These data indicate that all biological effects seen were dependent upon physical damage to the nerve, and were not associated with any other potential effects of the laser. Although we typically used cold to immobilize the flies, we also ablated and followed the response in animals that were immobilized by CO_2 to ensure that the method of immobilization did not impact the injury or response (Figure 3a). Additionally, changes in GFP seen upon axotomy were never seen in the uninjured contralateral wing, or in flies that were not ablated but otherwise treated identically to injured animals (Figure 3 and data not shown). Although it is not
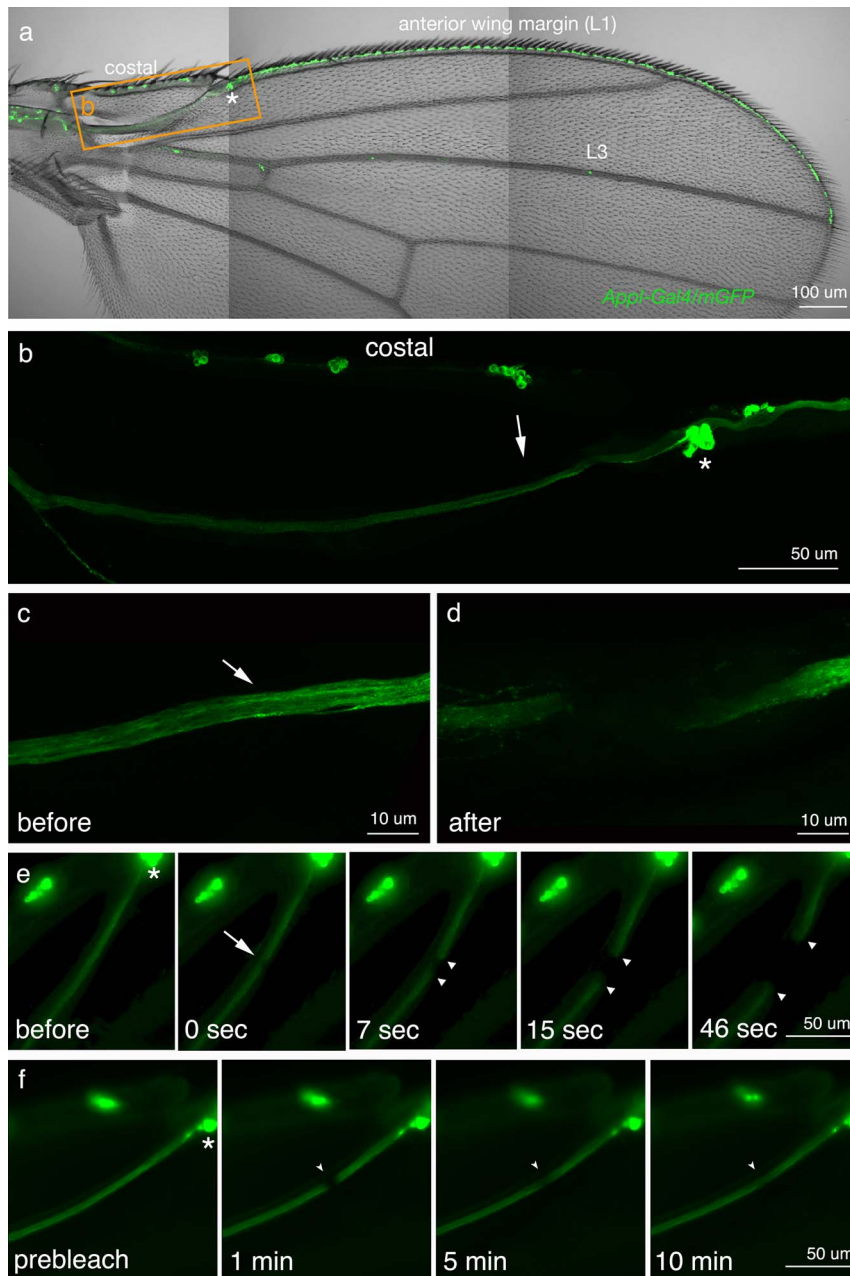
Figure 1 | Precise axon injury of the *Drosophila* wing nerve by laser ablation. (a) The nerve tract along the wing margin (L1), costal vein, and L3 are highlighted by mCD8-GFP using an *appl-GAL4* driver. The image is oriented with the wing tip to the right and the hinge region connected to the body to the left. The wing margin contains mechanosensory and chemosensory neurons from the point of intersection with the costal vein (asterisk) to the intersection with the tip of L3. The neurons send axonal projections in a nerve tract to the thorax. (b) Higher magnification of the region boxed in orange in (a), showing the nerve region where axotomy is performed. The last cluster of cells on the costal vein was used as a landmark to position the point of ablation (arrow). The last neural cell bodies along the wing margin are marked (asterisk). (c) High magnification of the nerve before laser ablation and (d) the same region after ablation. The nerve tract is precisely and completely severed with no visible damage to the surrounding tissue. (e) Time-course stills of laser ablation. The images are oriented with the first cell bodies of the wing margin on the top right (asterisk) and the nerve tract projecting to the thorax on the bottom left. The laser is centered (0 sec, arrow) using the last neural cell bodies on the costal vein (top left) as a landmark to ensure reproducibility. The laser is fired manually until the entire track is cut. Upon complete transection of the wing nerve tract, the two ends separate forming a gap (arrowheads, 7, 15, 46 sec). (f) Fast recovery of GFP after photobleaching of the wing nerve. Asterisk marks the last cell bodies of the wing margin. The region indicated by the arrowhead was bleached, and subsequent recovery of fluorescence was recorded at 1 min intervals to 10 min. Images in a and b are assembled from multiple confocal images. Images in (e) are still shots from Supplementary Movie 1. Images in (f) are epifluorescence images on a Leica DM6000B. Genotype *yw appl-GAL4; UAS-GAL4 UAS-mCD8-GFP/+*.

possible to immunostain within the wing[19,23], we confirmed that the GFP pattern mimicked the axonal response with differential interference contrast (DIC) microscopy (Supplementary Figure S2). These findings indicate a robust and reproducible neural regenerative response that occurred only upon precise axonal transection.

A scar at the injury site. Our studies revealed formation of a noticeable scar at the injury site by prominent deposition of pigment (Figure 2a–d, g). On d1, pigment was typically restricted to a small area and light in color; the area of pigment increased with time and darkened. By d3, deposition of pigment at the injury site
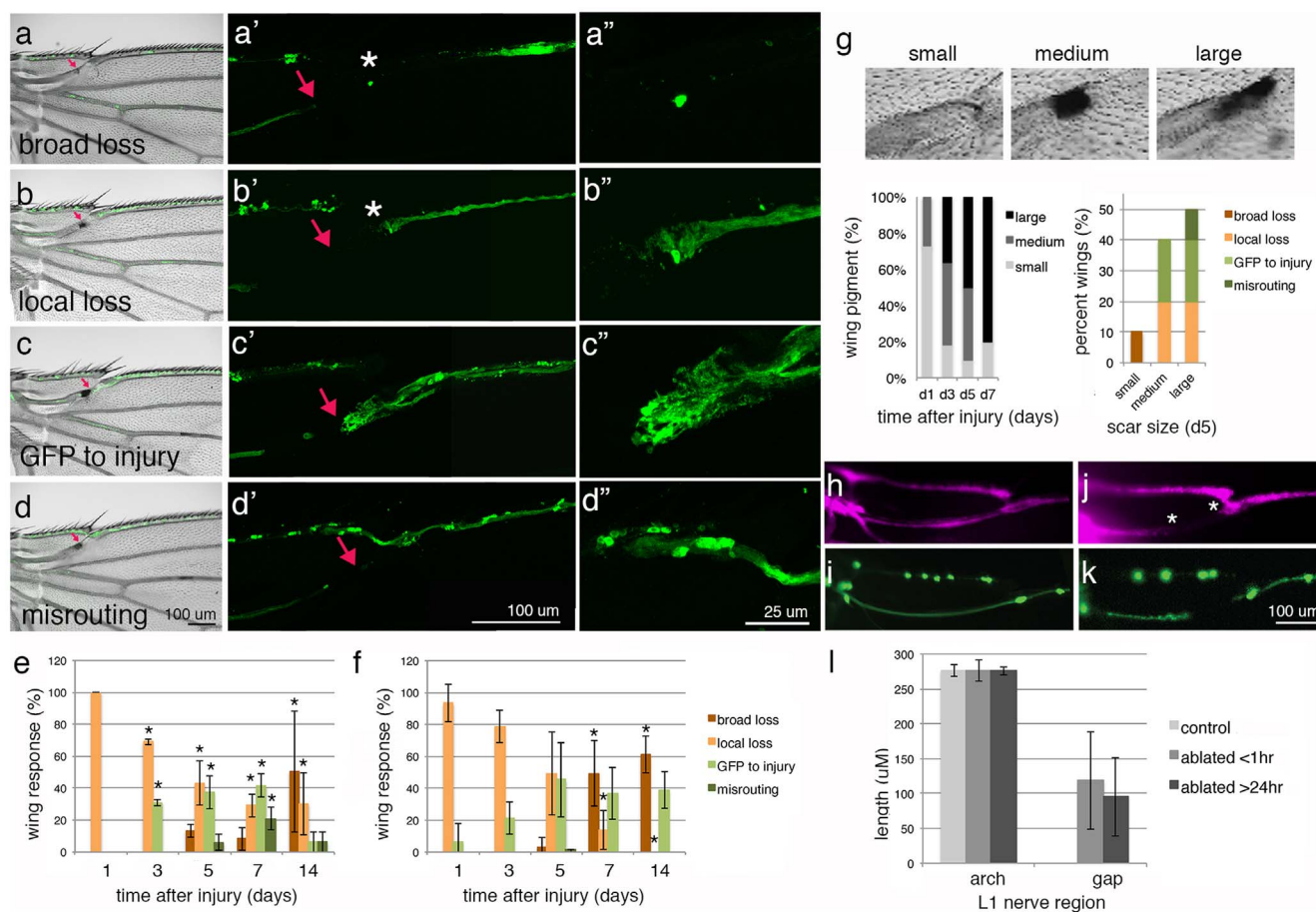
Figure 2 | **Axotomy of the wing nerve induces a regenerative response characterized by axonal growth, formation of a scar and blockage to hemolymph flow.** (a–d, a'–d', a''–d'') Representative images of wing nerve response at d7 after ablation. Nerve tract highlighted by mCD8-GFP with *appl-GAL4*. (a–d) Wing cuticle and the nervous system. (a'–d') Response of neurons highlighted with mGFP, and (a''–d'') magnified view of neural endings. Assembled confocal images. On d7 after ablation the wing nerve displays signs of regeneration and formation of a scar at the injury site (magenta arrow). Wings response categories: (a–a'') Broad loss, the first neural cell bodies along L1 are indicated (white asterisk); (b–b'') Local Loss; (c–c'') GFP to Injury; (d–d'') Misrouting. (e and f) Quantification of response categories after ablation of (e) 6h and (f) 1d (24 h) adults. Mean ± SD. Asterisks (*) mark those biological classes statistically different (*P* < 0.05 or less) from 1 d category of that biological class in each graph. ANOVA for significance followed by Tukey's multiple comparison test. 3 sets of wings/time point; n=7–23 wings/set. (g) Quantification of the scar at the injury site. Top panels, scars. Quantification, repeated 3 times per time point. Left, scar sizes for a single set of animals at each time point (d1-d3 n=11, d7 n=10 wings). Right, correlation between scar size and biological class for d5 animals (11 wings). (h and j) Dextran dye flow is blocked around injury site. Live imaged animals. (h) Control wing injected with Dextran shows dye in the wing arch. (j) Ablated wing showing exclusion of dye in the arch. Dye does not penetrate between white asterisks. (i and k) GFP in ablated wing (h and i) and control wing (j and k). (l) Quantification of the arch length and gap in the arch, Dextran is excluded from the arch after ablation; exclusion takes place immediately upon ablation (exclusion within 2–3 min, <1h class). Mean ± SD. Control, 17 wings; <1h, 16 wings; >24h, 23 wings. Bar in d panel, 100 μm for a–d. Bar in d', 100 μm for a'–d'. Bar in d'', 25 μm for a'' to d''. Bar in k, 100 μm for h–k. Genotype *yw appl-GAL4; UAS-GAL4, UAS-mCD8-GFP/+*.

ranged in size, such that by d7 the majority of wings had large scars (Figure 2g). Scar formation only occurred in wings where the nerve tract was severed, and was never seen in the uninjured contralateral wing or in flies that did not undergo ablation but were otherwise similarly treated (Figure 3). Importantly, scar formation was not seen in wings where the laser was fired inside the L1 vein without injury to the axon bundle (Figure 3). The location of pigment deposition coincided with the area that axons appeared unable to cross. Wings with axonal growth displayed axonal extension to the scar (GFP to Injury category) or alternatively, the projections invaded the costal vein (Misrouting). We assessed the size of the scar and the biological response in one set of wings at 5d. These data showed no consistent trend of scar size with biological response, although the Misrouting class was associated with a large scar. This finding raised the possibility that the growing axons were not able to cross the injury site, and that the scar may be or reflect a physical or repulsive chemical barrier.

To determine whether the scar was a physical barrier, we injected low molecular weight Texas Red-labeled Dextrans (3kDa) into flies immobilized on agarose (Supplementary Figure S1) and monitored dye filling along the wing veins by high-speed time-lapse microscopy. In control wings, dye followed the characteristic pattern along the longitudinal veins. We first looked at the effect of the scar by injecting dye into animals >7d, after a visible scar had formed. With the exception of a few animals, dye was blocked from the injury site, and was also blocked from the L1 arch region far from the injury site, indicating an effect far larger than the physically visible pigment (Figure 2h–l). To define the timing of dye exclusion, we injected dye into animals immediately following ablation. Surprisingly, dye exclusion was already present. The extent of occlusion within 1h of ablation was the same as in older animals (119 ± 70 μm <1h, vs 96 ± 56 μm >24h; the length of the L1 arch averaging 270 μm; Figure 2l). These data indicate that the physical pigment-marked scar is not necessary for dye exclusion from the injury site.
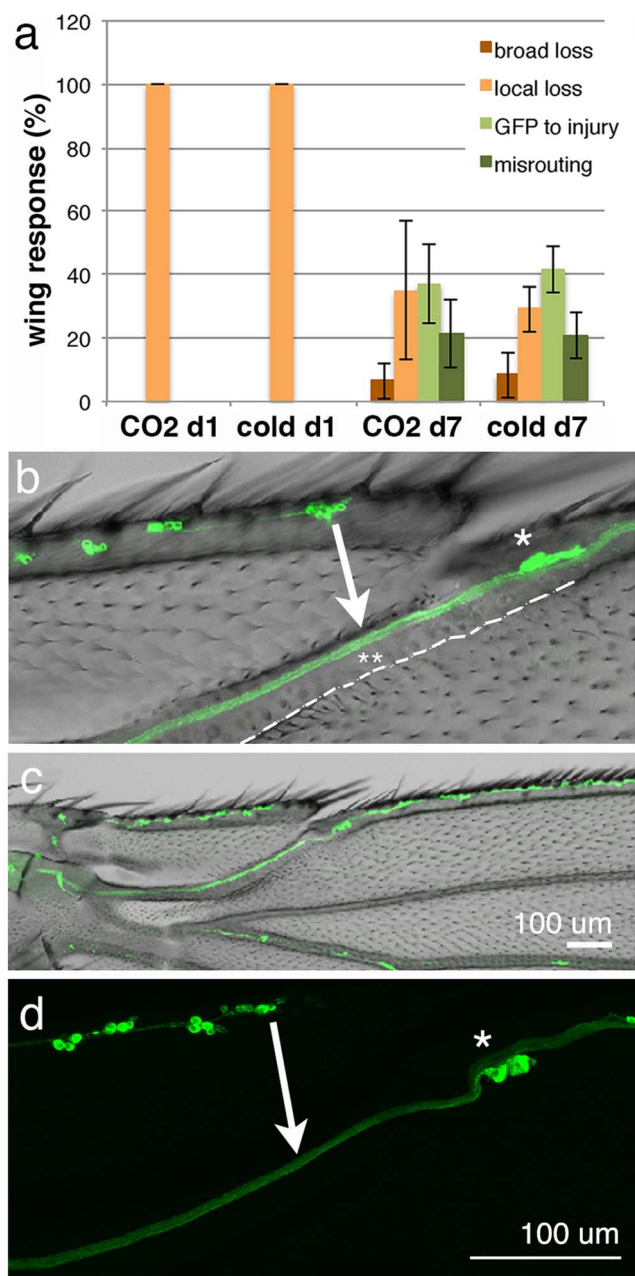
Figure 3 | Biological response to injury requires nerve ablation.
(a) Quantification of the wing response to axotomy by immobilizing flies using CO_2 versus ice. The response at d1 and d7 after injury is not different. Mean $\pm$ SD; 3 sets of wings/condition and time; n=10 wings/set.
(b–d) Firing the laser inside the L1 vein without axonal damage does not lead to changes in GFP or scar formation. (b) Wing region of interest showing the axonal tract and the L1 vein boundary (marked by white line). For control experiments to assess whether any responses occurred upon mock ablation, the laser was fired inside the vein using the same strength as for nerve ablations at the site marked by double asterisk. (c) No scar is seen in wings after mock ablations. 7d wing. (d) Higher magnification assembled confocal views of the neuronal GFP of wings in c, which remains unchanged after mock ablation. First L1 neural cell bodies, single asterisk. Bar in d, 100 μm for b, d. Bar in c, 100 μm for c. Genotype *yw appl-GAL4; UAS-GAL4, UAS-mCD8-GFP/+*.

Age dependence of the regenerative response. Our initial studies were on 6h adults, and we were interested in whether the response changed with age. We therefore injured flies that were 1d and 3d old, and followed their response and recovery over time. This revealed

that a regenerative response was indeed present in older injured animals, although with an overall diminished capacity (Figure 2f and data not shown). For 1d animals compared to the earlier timepoint of 6h, the response was generally similar, while the 7d and 14d responses showed more widespread loss of GFP extending from the injury site along the wing margin. Older animals, however, still showed considerable regrowth, with the GFP to Injury category remaining robust even at 14d (39 $\pm$ 12%; Figure 2f). Animals injured at 3d also showed Misrouting, but this required a longer time period (21d–30d). These data indicate that 6h compared to 3d animals show a switch in response to injury within the first two weeks: 6h flies showed a peak window of regenerative capacity at 7d post-injury, while 3d animals showed peak regrowth occurring later (21d). Thus, older flies retain the capacity to regenerate, but do so at a slower pace. In these studies, we also noted that neurons along the wing margin underwent an age-associated deterioration when comparing 3d to ~35–50d animals. This response consisted of progressive disorganization in morphology of the axon bundle with a frayed appearance, anomalies in the position of the neural bodies along the axonal tract, an increase in pigmentation along the margin, and loss of the GFP in regions of the nerve. These observations made time course studies of older animals difficult, thus we focused our studies on 6h animals where we could assess the regenerative response within 1 week.

A rapid, transient, long range impact to the cytoskeleton in injured axons. A pivotal step during regeneration is the propagation of the injury signal back to the cell body, and subsequent transportation of membranes and cytoskeletal elements to the injury site for recovery[24]. To initiate studies to address this, we investigated whether changes to the microtubule cytoskeletal network were notable upon injury. To do this, we used EB1-RFP to visualize the microtubules; EB1 binds the continuously expanding and retracting microtubule plus ends, positioned at the distal tip in axons[16,25,26]. Before injury, microtubule labeling by EB1-RFP appeared smooth throughout the entire length of the axons, from their cell bodies at the tip of the wing down to the projections near the thorax (Figure 4a,b).

Upon axotomy, signal was immediately lost around the injury site, suggesting a rapid breakdown of the microtubule network. By 5 min, the EB1 signal started changing from smooth labeling to a more diffuse, spotted globular appearance on both sides of the axonal ends at the injury site. The spotted labeling of EB1, indicative of an impact on microtubules, propagated along the margin toward the wing tip: by 2h, EB1-RFP had a spotted appearance extending to the intersection with L2 (Figure 4a timeline, 4c). Thus, an impact on microtubule organization was detectable along the whole length of the L1 nerve bundle, including those cell bodies located at great distance from the site of injury (the wing is ~2 mm in length). Intriguingly, the disruption was transient: 1d after injury, EB1-RFP regained a smooth appearance (Figure 4d). In contrast to the temporally transient and spatially long-range re-organization of microtubules in the axons along the margin, the severed axonal ends showed only local changes to EB1 near the injury site that did not recover (Supplementary Figure S3). Loss of the EB1 signal started at 1d and propagated down the axonal ends toward the thorax such that by d7 no signal was detected.

We also examined the actin signal using Lifeact that labels filamentous actin[27,28]. Although this signal was more difficult to detect, given coincidence with autofluorescence of the wing, we discerned that the Lifeact dissipated rapidly within the nerve ends upon ablation (Figure 4e–h). The signal did not recover at 1d like the EB1-FFP signal (data not shown); however, at later time points (7d), we saw the signal at the axonal ends coincident with neural membrane GFP (Figure 4i).

We also examined the severed axonal ends for signs of fragmentation indicative of Wallerian degeneration. Although the GFP signal diminished over time, we could not detect fragmentation due to the
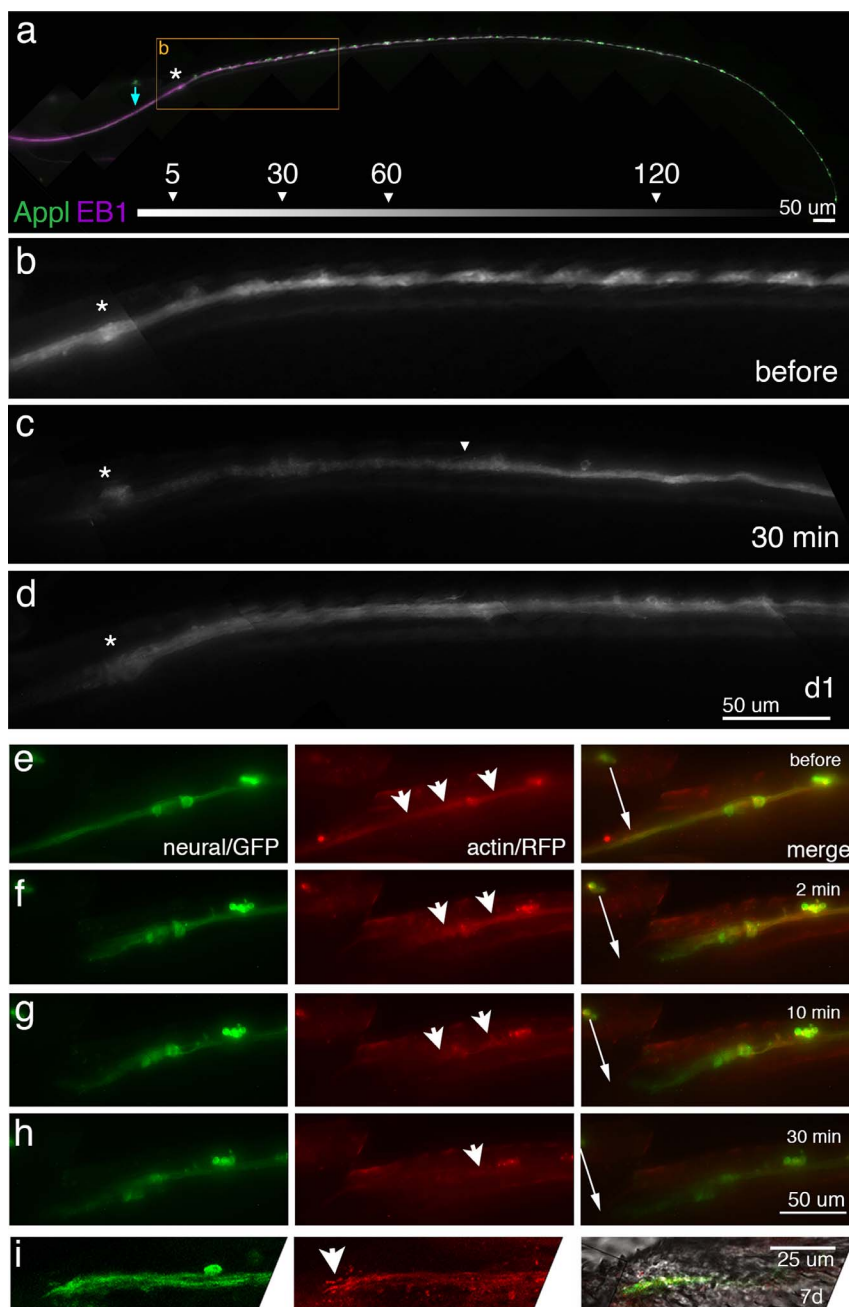
Figure 4 | Axotomy results in widespread changes to the cytoskeleton. Live imaging of the wing to detect (a–d) microtubule changes with EB1-RFP and (e–i) actin changes with Lifeact-Ruby. (a–d) The L1 nerve is highlighted by mCD8-GFP and EB1-RFP, a protein that binds microtubule plus ends. Wing tip, to the right. Last cell bodies of the margin (asterisk). Blue arrow, ablation site. Time line at bottom of panel is time in min of progression of disruption of EB1-RFP signal following severing of the nerve by laser ablation. (a) Prior to injury, EB1-RFP labeling is smooth and increases in intensity as the tract thickens. (b) A higher magnification of the region in the orange box in (a). (c) 30 min following ablation. The EB1-RFP signal changes from a smooth labeling of the axons to a globular appearance with time; this morphological change starts near the point of ablation and progresses retrogradely along the axons towards the tip of the wing. The arrowhead marks closest point where signal remains smooth at specified min post ablation. (d) By 1d after injury, the EB1-RFP signal has recovered, such that now the only visible change is loss of signal near the injury site. Assembled epifluorescence images of live wings on a Leica DM6000B. Bar in a, 50 μm for a. Bar in d, 50 μm for b–d. Genotype *yw appl-GAL4/UAS-EB1-RFP; UAS-GAL4, UAS-mCD8-GFP/+*. (e–h) Live imaging of neurons highlighted with mCD8-GFP and Lifeact-Ruby for filamentous actin in red. i) Confocal fixed images of 7d animals. e–h, filamentous actin signal, highlighted in red in middle panels is smooth before ablation, but rapidly dissipates upon nerve transection (arrow heads highlight actin signal, arrow indicates site of transection). The actin signal has not recovered by 1d (data not shown), but i) by 3 d is coincident with the neural signal. In i, merged panel includes bright field to visualize the pigmented scar. White arrowhead highlights restored Lifeact-Ruby signal. Scale bar in right panel of h, is 50 μm for e–h, and 25 μm for i. Genotype *yw appl-GAL4/UAS-Lifeact-Ruby; UAS-mCD8-GFP/+*.

large number of axons that constitute the tract. Analysis of MARCM clones of ~20–50 neurons, however, revealed striking fragmentation followed by loss of the GFP signal indicative of clearing (Supplemental Figure S4). GFP loss in the severed projections was delayed by Wld[s] (data not shown). These data indicate that, after axon damage, the microtubule network falls apart in the distal sev-

ered axonal ends, and that cytoskeleton collapse precedes axonal membrane clearance.

Migration and accumulation of hemocytes around injured axons. In metazoans, macrophages are highly motile cells that clear pathogens and damaged cells after infection or wounding[29]. Hemocytes are the macrophage equivalent in *Drosophila*[30,31]. To investigate a potential hemocytic response upon neural injury, we transected the nerve bundle and imaged wings live with the neuronal and hemocyte components differentially labeled. The nerve was labeled in green with mGFP and hemocytes in red with mCD8-ChRFP using a *Hemese* driver *He-GAL4* (Figure 5). Normally, hemocytes are not abundant in the wing region and show minimal movement within the L1 vein (Figure 5a, e, i–j; Supplementary Movie 2). Immediately upon nerve transection (up to 30 min followed with live imaging), circulating hemocytes inside the wing veins showed a rapid local movement response (Figure 5k–l; Supplementary Movies 3, 4). The response required neural damage, since firing the laser within the L1 vein without injuring the axons had no effect. The movement of hemocytes appeared local and non-directional over this short time course (Figure 5l). Over longer periods (d1–d7 after injury), an accumulation of hemocytes occurred around the distal axonal ends undergoing degeneration (Figure 5b–d, f–h).

Glial response to axotomy. We likewise labeled the neuronal and glial components of the nerve using two expression systems (GAL4/UAS and GAD/lexA) with the nerve in GFP and glia labeled with a repo driver in RFP. In live imaging, upon axonal transection the glial signal was cleared at the site of ablation, although the gap in signal was not as great as with the nerve in GFP. Moreover, despite the snapping back of axons and a gap in the GFP due to axotomy, this was not seen in the glial signal, such that loss of RFP was only

detectable in a small gap at the site of laser ablation (Figure 6a–c). We detected no consistent change in intensity of the glial membrane signal immediately or over time, in contrast to the documented response along severed axonal distal ends in injury models where the neuronal cell bodies are removed and regeneration is not possible (see[20,23]). The only consistent response of glia at later times was absence of signal coincident with axonal loss, indicating an interdependence of the glial and neuronal signals (Figure 6d, e).

Modulation of the JNK signaling pathway increases regeneration. Our studies indicated that the wing nerve in the adult animal can recover upon severe injury and undergo a regenerative response. To extend these findings, we initiated a genetic screen for modulators that promote regrowth. The nerve was labeled in green with one expression system (GAD/LexA), and transgenes of choice were expressed conditionally using a drug-dependent GeneSwitch (GS) GAL4 system[32] to avoid developmental effects and identify pathways that can impact regeneration after injury. The transgenes were expressed in all cells using tubulin-GS, or selectively in neurons with elav-GS. Adult flies were collected, aged to 6h on drug-containing (RU486) food to turn on the transgene of interest or on vehicle (EtOH) as control, the wing margin nerve bundle was severed by laser ablation, and animals were aged further on food containing drug or vehicle. Robust conditional transgene expression was seen by 6h (data not shown; see[32]).

In screening transgenes that modulate signaling pathways, we found that downregulation of the c-Jun N-terminal kinase (JNK) pathway using a dominant negative form of *basket* (*UAS-bsk-DN*) resulted in robust enhancement of the regenerative response (Figure 7). As before, animals at 7d on vehicle food showed the characteristic axonal response of extending projections not capable of crossing the injury site, such that they stalled or misrouted as they
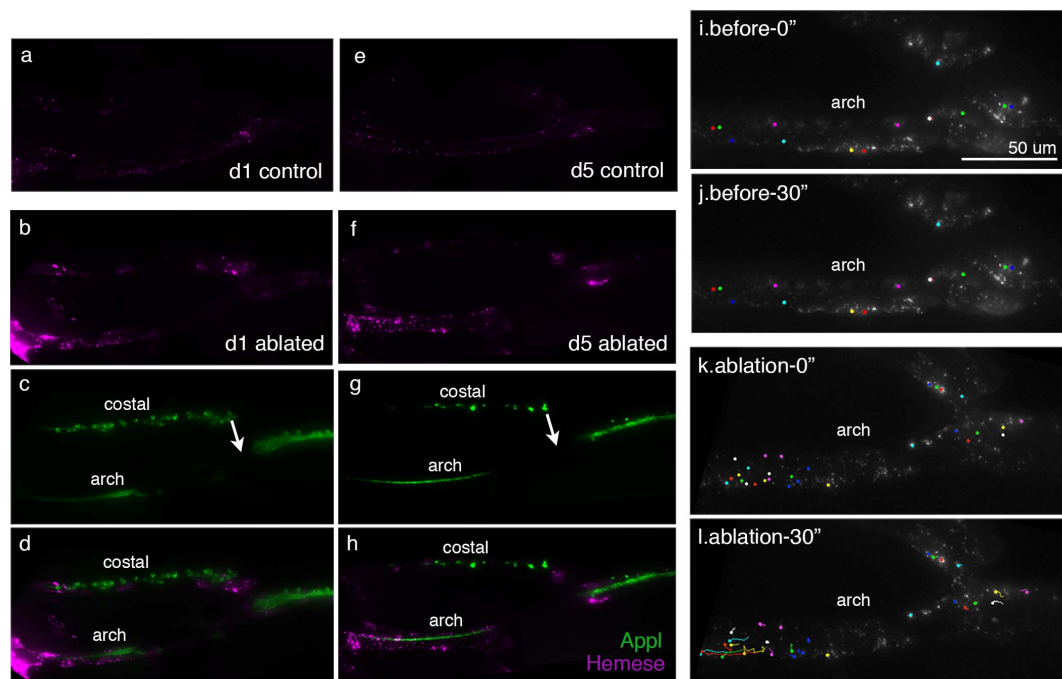

Figure 5 | Hemocytes become motile upon neuronal injury and accumulate around degenerating distal axons. Wing nerve is labeled by mCD8-GFP and hemocytes labeled by mCD8-ChRFP. Images of the costal and arch area. Wing tip to the right. Axotomy site (arrow). (a, e) mCD8-ChRFP image of control wings showing that hemocytes show minimal accumulation normally. (b–d) d1 and (f–h) d7 after ablation. Hemocytes accumulate around degenerating distal axons. (i–l) Frames from live imaging movies of hemotypes. Movement of hemocytes is tracked in the 30'' long movie; shown are frames at start and end. (i,j) Hemocytes in control animals are not highly motile. (k,l) Hemocytes are motile immediately after axotomy and move towards distal axonal ends. Assembled panels of live imaged animals. Data shown are representative of at least three repetitions of at least three independent experiments; controls with no motion included animals where the laser was fired into the vein in absence of nerve damage. Bar in i, 50 μm for i–l. Genotype *yw; LexAop-mCD8-GFP/+; nSyb-lexA-GAD elav-GS/He-GAL4 UAS-mChRFP*.
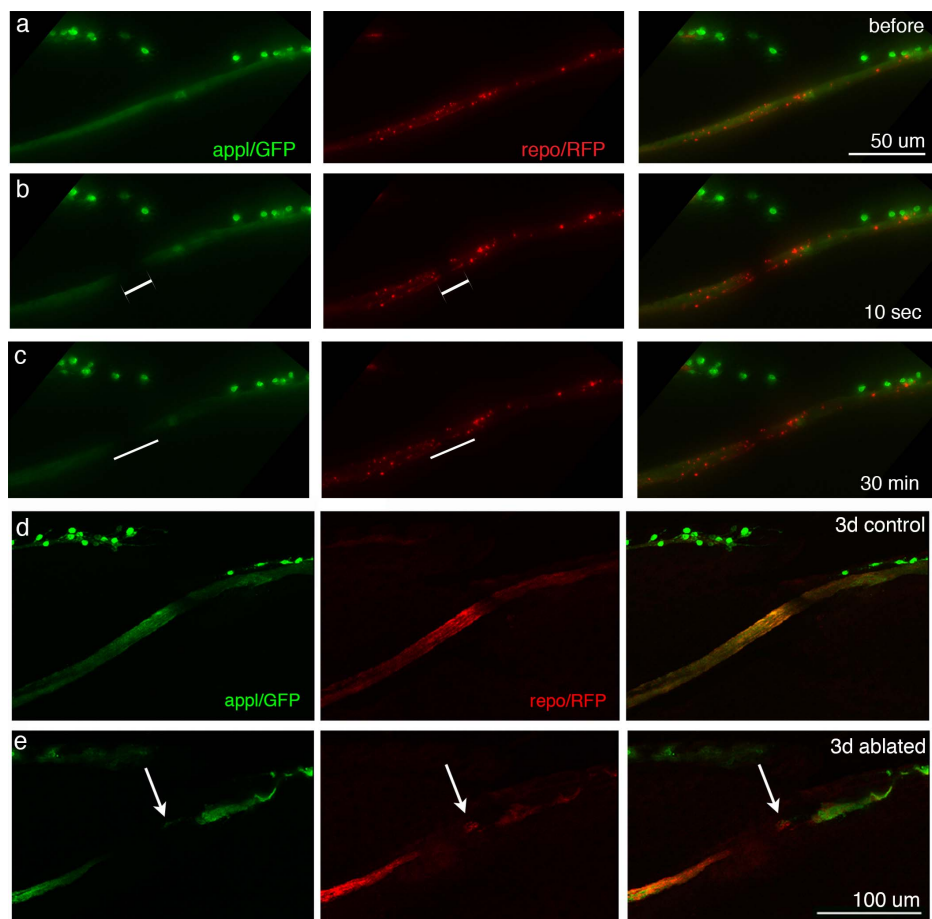
Figure 6 | Glial response upon injury. (a–c) Live imaging of the glial response to nerve severing. The L1 nerve is highlighted by mCD8-GFP and the glial signal in mCD8-chRFP. In live imaging, the glial signal showed puncta. Wing tip, to the right. Arrow, ablation site. White line, gap in axonal projection due to laser severing of the tract. (a) Prior to injury, the glial signal indicates that the glia wrap the neurons. (b) Upon ablation, a gap (white bar) forms in the nerve. A gap is also seen in the glial signal. (c) 30 min after ablation, the neural gap has progressed to become slightly wider, whereas the glial gap remains similar to immediate time points. Epifluorescence of live wings on a Leica DM6000B. Bar in a, right panel, 50 μm for a–c. Genotype *yw*; *LexAop-mCD8-GFP/+; nSyb-lexA-GAD elavGS/repo-GAL4 UAS-mCD8-ChRFP*. (d-e) Fixed wings for neural and glial signals. The L1 nerve is highlighted by mCD8-GFP and the glial signal in mCD8-RFP. Note that although the glial signal is punctate in live imaging (a–d), it is smooth upon fixation. Wing tip, to the right. (d) Control wings show glial signal coincident with the neural signal indicating that the glia wrap the nerve. (e) 3 d post-injury, the glial signal is largely coincident with the neural signal. No consistent changes in intensity of the glial signal were seen with time. Arrow, ablation site. Bar in e, right panel, 100 μm for d, e. Confocal images. Genotype *yw*; *LexAop-mCD8-GFP/+; nSyb-lexA-GAD elavGS/repo-GAL4 UAS-mCD8-ChRFP*.

reached the scar. In striking contrast, in flies expressing Bsk-DN, 49 ± 22% (mean ± SD) of animals showed no GFP signal loss beyond the site of nerve injury, and in 22 ± 4% (mean ± SD) of animals the axons showed a new response, Crossed Injury (Fig. 7a, c)—a response never seen in our study thus far. In these animals, the nerve axonal tract had been completely severed with the laser.

The nerve growth response was similar whether Bsk-DN was expressed ubiquitously with tubulin-GS, or selectively in neurons with elav-GS, indicating the enhanced growth was dependent on altering neuronal signaling and not the environment (Figure 7b). The Bsk-DN expressing wings also showed a marked decrease in size of the pigmented scar (Figure 7d, e). This indicated a correlation in size of the scar and ability for axons to cross the injury site, although Dextran dye exclusion studies indicated that dye was occluded from the injury region of the arch similar to control ablated animals (data not shown; see Figure 2l). These data indicate that downregulation of the JNK signaling pathway in the neurons of the adult wing stimulates dramatic regrowth, including the ability to route through regions previously appearing as a barrier. Consistent with this, upregulation of the JNK pathway with a constitutively active *hemipterous* (Hep-CA) transgene resulted in the opposite response, with no Crossing Injury or Misrouting categories,

a dramatic increase in the Broad Loss category and only large pigment scars (Figure 7a, d).

Discussion
We desired a method to injure axonal tracts in the living adult animal while keeping the neural cell bodies intact and animals alive and well, thus allowing us to monitor the potential for neural recovery with age. This approach has significant advantages over other paradigms[19,20,23]: it allows study of the biological response in neurons with adult-stage growth capacity; it is performed *in situ*, allowing study of the biological response in the native, *in vivo* context; the tract is recognizable, allowing analysis of the response of the same set of neurons reproducibly and repeatedly; the response can be visualized multiple times in the same animal over time; one can follow the response of different sets of cells using the variety of available gene driver systems and labeled tags; and the tract is extremely large, being comprised of ~225 axons that project over a very long distance. Limitations include the need to tag proteins *in vivo* with fluorescent markers, and, at this time, inability to readily distinguish existing nerve projections that have been injured from those of new growth. This preparation thus has significant advantages that make it a strong complement to existing paradigms.
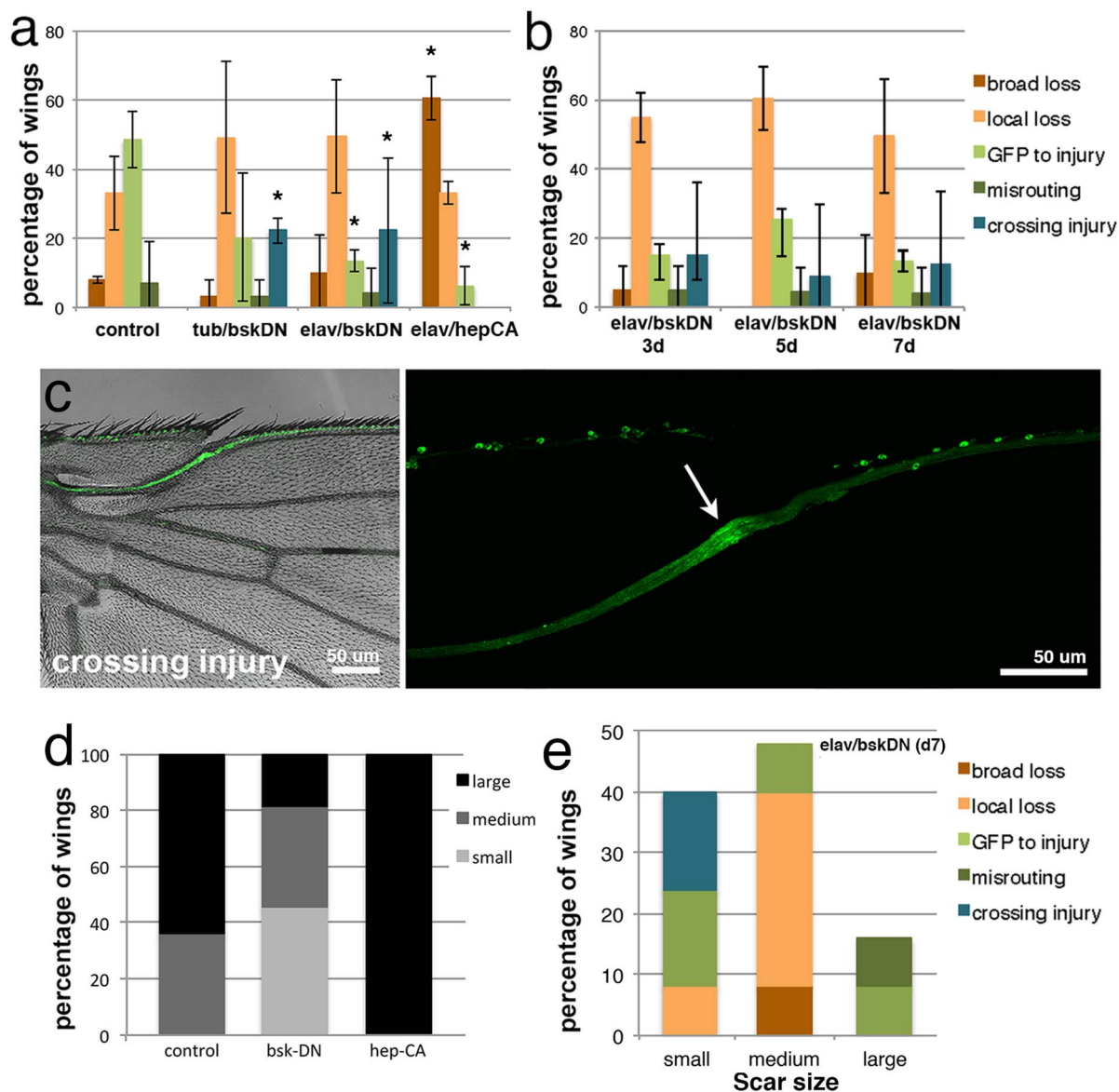
Figure 7 | Downregulation of the JNK signaling pathway in neurons increases regeneration and promotes axonal crossing through the injury site.
(a, b) Quantification of the neural response to axotomy in animals conditionally expressing BskDN ubiquitously (tub) or selectively in neurons (elav) or HepCA selectively in neurons (elav). Response at (a) 7d and (b) a time course of neural specific expression showing the acceleration of the response and that the new class of crossing injury is present already by 3d (compare to Fig. 2e). Mean ± SD. (n=3 sets of animals each time point; 6–13 wings/set). In a, asterisks (*) mark those biological classes statistically different ($P<0.05$ or less) from control category of that biological class in each graph. Anova for significance followed by Tukey's multiple comparison test. In b, none of the percentages of each biological class are significantly different across genotypes. Thus, the distribution of biological classes at 3d is not significantly different than at 5d or 7d. (c) Representative wing showing axonal re-growth through the injury site. Confocal with bright field (left), and assembled confocal image (right). (d) Quantitation of size of pigment scar in normal, BskDN animals, and HepCA expressed with elav-GS, in one set of animals for each genotype at 7d (n=6–8 wings/genotype) (e) Distribution of scar sizes with biological class for one set of animals of elav/BskDN d7 (11 wings). The Crossing Injury class is correlated with a small scar, whereas the misrouting is associated with a large scar. Dextran dye injections show dye was occluded from the arch region in Bsk-DN animals in a manner similar to controls (data not shown; see Fig 2l). Bars in c, 50 μm. Genotype *yw UAS-bskDN or UAS-hepCA; LexAop-mCD8-GFP/+; nSyb-lexA-GAD elav-GS/+.*

Our initial experiments following the neural GFP pattern revealed a minimal response within the first several days. Intriguingly, EB1-RFP—a cytoskeletal probe for the microtubule network—showed an immediate impact on the injured axons with a rearranged signal that propagated along the entire length of the wing margin, to the furthest nuclei at the tip. This demonstrates a fast response along all the neurons, even those far from the site of damage. Lifeact to label filamentous actin also displayed an immediate impact to the actin cytoskeleton network. Hemocytes around the neural injury site also responded with a motility response, and Dextran studies revealed immediate dye occlusion through the arch. Rigorous controls con-

firmed that these responses all required physical damage to the nerve bundle. The development of the pigmented scar on the wing cuticle also required neural damage. This scar darkened over time, perhaps reflecting a block around the ablation region as supported by dye occlusion experiments. Interestingly, mitigating JNK signaling with Bsk-DN in the neurons also mitigated the size of this scar. Previous studies with adult *Drosophila* models have not reported a visual scar[14,20].

In *Drosophila* and *C. elegans* a number of studies have revealed insight into neural regrowth pathways[3,5,12,16,25]. These are dependent on both stage (developing versus adult), as well as neuron type.

Despite some exceptions (see[33]), specific pathways critical to neural regrowth do not appear to be universal to all neurons and stages; rather, neuron-specific pathways have been revealed. Our approach to selectively manipulate pathways in the adult stage and with different cell-specific drivers will allow extension of such studies to other associated cells (hemocytes, glia)[34]. The ability to temporally regulate pathways may allow identification of pathways that can be manipulated to achieve regrowth long after the time of neural injury. The JNK pathway was inhibitory to growth after injury in a neural intrinsic manner. JNK has been shown important for induction of Wallerian degeneration during axonal injury in the adult fly olfactory system and in dorsal root ganglion cells[35,36]. In contrast, however, the JNK pathway promotes neural growth in explants of the adult fly central brain tissue and in growth upon traumatic brain injury[14,37]. In the developmental context, JNK is important for axon formation[16,38,39] and helps to drive axon guidance[40]; it is also associated with the regenerative response[41]. A role of the JNK pathway to inhibit regrowth in a neuronal intrinsic manner occurs in motor neurons in *C. elegans*[42]. Interestingly, *C. elegans* neurons also display increased neurite projections with age, and reduction in JNK signaling dramatically promotes this activity as well[43,44].

Inhibition of the JNK pathway in wing neurons led to a new response of crossing the injury site. Analysis of all categories suggests that members of the GFP to Injury class became Crossing Injury, indicating an ability to navigate the injured site. A kink, as if to avoid the precise site of injury, was also commonly seen (see Figure 7c). Interestingly, there was no change to dye occlusion from the arch, indicating that manipulation of JNK signaling promoted navigation of growing axons through the scar. As the pigmented scar was also smaller, the scar appears stimulated by damage of the neural bundle; pathways that mitigate the scar may also promote the ability of the axons to navigate through an injury. Although we do not know the mechanism of the JNK pathway in the context of our studies, it has been noted to serve as a gatekeeper for organelles, allowing rapid mobilization of organelles/vesicles along projections for rapid recovery and growth upon injury[42,45]. For these neurons, we also found that regenerative capacity is retained in older animals, albeit delayed. Thus, identification of gene pathways that promote the speed of regrowth may also dramatically impact age-associated decline.

Methods

Drosophila stocks. Flies were grown on standard cornmeal, molasses food at 25°C. Males were typically used. Strains included *appl-GAL4*, *Hemese-GAL4*, *repo-GAL4*, *UAS-GAL4*, *UAS-mCD8-GFP*, *UAS-mCD8-ChRFP*, and *LexAop-mCD8-GFP*, *UAS-bskDN*, *UAS-hepCA*, and *UAS-Lifeact-Ruby*[27,28] (Bloomington *Drosophila* Stock Center (BDSC), Indiana University (Bloomington, IN)). Other lines were *UAS-EB1-RFP* (Dr. M. Rolls, U. Michigan, Ann Arbor, MI), LexA-CD4-GFP and LexA/nSynaptobrevin[46], elav-GS[32], tubulin-GS (Dr. Scott Pletcher, U Michigan, Ann Arbor, MI). Animals were collected over a 2h period then aged 5h for 6h, 24h for 1d, and 72h for 3d animals. Flies on RU486 (Mifepristone, Sigma Aldrich, cat# M8046) were maintained on food supplemented with drug[32]. Briefly, for each food vial, 50 ul of RU486 stock solution [4.0 mg/ml in 100% ethanol] was pipetted onto the medium and allowed to penetrate the food overnight. UAS-transgenes showed robust expression throughout the wing within 18h of being placed on RU486-containing food, and visible transgene expression (hinge region close to the body of animal) by 6h[32,47]. Bottles of animals were cleared, collected over a 2h period and put on RU486 or vehicle food and aged for nerve injury.

Laser axotomy. *Laser system.* Axotomy was performed with a MicroPoint laser system[48], mounted to a Leica DM6000B compound microscope. The pulsed nitrogen pumped tunable dye laser was optimized to efficiently cut nerves on adult *Drosophila*. The dye cell was filled with Coumarin 440 and a dichroic for GFP was used for ablations. A wavelength of 440 nm was found optimal for ablation in adult flies, and of the wing nerve. The dichroic for GFP was found best for ablations on adult *Drosophila* due to the autofluorescence of the cuticle. The laser was fired using a foot pedal. Ablations were done manually without the use of a camera to guide the laser due to the large number of axons and width of the target nerve. Ablations were performed in the absence of damage: excessive power causing damage was readily seen as blebbing or physical damage to the wing. The Leica DM6000B microscope was equipped with a 10× dry objective for finding the target to be ablated and a 63× water-dipping lens for ablation itself.

Immobilization of the flies. Flies were mounted on agarose and kept immobilized at 4°C. A solution of 2% low melting agarose (SeaPlaque, Lonza) in ddH₂O was prepared, melted and acclimated to 55°C in a water bath. Flies were anesthetized and oriented ventral side up on a CO₂ pad. Agarose was poured into a glass slide with a mounted plastic chamber (Lab-Tek^R II Chamber slide, Nalge Nunc International Corp.). The flies were mounted with the wings flat on the agarose using tweezers with blunt edges. 10 flies were lined up per slide, then the slide was quickly cooled on an Eppendorf PCR Cooler Iceless Cold Pack that had been chilled to −20°C. Once the agarose had solidified, the slides with mounted flies were transferred to ice or 4°C refrigerator until ablation. Ablations were performed right away, within a 2-hr window.

Neuronal injury of the wing nerve. The prepared slides were placed on the microscope stage and the flies were submerged in ddH₂O. Each wing to be ablated was brought into focus using the 10× objective and the ablation target area was centered near the crosshairs of the eyepiece. The axonal tract underneath the first cluster of costal cell bodies was brought into focus after switching to the 63× water-dipping lens. The laser was fired while the stage was moved incrementally to cut the entire width of the axonal tract. Typically 5–6 pulses of the laser were needed to sever the nerve bundle. Complete transection of the wing nerve was achieved with nearly 100% success if the wing was mounted properly (flat and away from the body). Flies with incomplete transection of the nerve with up to 12 laser pulses were discarded. Initial studies comparing laser ablation with confocal images of the wing immediately after ablation confirmed that the nerve snapped apart only upon complete transection: thus when the nerve was seen to snap apart, we were certain that the projection had been completely severed. Animals where the nerve did not snap apart were discarded. Axotomized flies were gently lifted from the agarose using a paintbrush, excess water was removed with Kimwipe and the fly paced in an individual vial. Only one wing per fly was ablated, the other wing served as the uninjured control. Wings from unablated flies that were otherwise mounted as if for ablation were also scored to ensure that unilateral ablation had no effects on the contralateral side. Flies were allowed to recover with the vial horizontal, then animals aged to desired time points at 25°C, switching to new food vials 3× per week.

Analysis of wing nerve response to injury. Animals could be mounted on agarose and subjected to injury then recovered, or could be followed live for response to injury using tagged transgenes for a maximum of 2 h with no impact on animal viability or survival. Following mounting and recovery from ablation, animals could be mounted a second time and scored for a live response. Mounting the animals twice was robustly tolerated, but mounting more than twice resulted in high mortality. Therefore, animals were live mounted at most twice. For scoring the wing response in fixed tissue, wings were dissected from the animal, mounted and imaged. Wings were fixed by preparing a 1 : 1 mixture of n-heptane and 2.5% paraformaldehyde in PBS, and using the top layer (heptane) as a fixative for 2h at RT. Subsequently, wings were subjected to 3 quick washes in 1% Tween-20 in PBS, one wash for 30 min, then 3 quick washes in PBS, one wash in PBS for 30 minutes, then mounted (Vectashield Mounting Medium, Vector Laboratories). Scoring of the response to injury was typically done on a Leica DM6000B, and in select situations, by detailed analysis on a Leica TCS-SP5 confocal microscope for detailed assessment. Because of its exceptional size, confocal analysis of the wing required multiple scans at high magnification and detailed manual assembly of individual image panels. Lower power images (e.g., Fig. 3a–d) are single image panels; higher power images are manual assemblies of 4–5 confocal scans. Images were processed using the Leica Application Suite (LAS) microscope software. For live imaging (movies, hemocyte motility, EB1-RFP labeling studies), animals were mounted and imaged on a Leica DM6000B microscope using Leica software (LAS AF 3.1.0). Data shown are representative of at least three independent repeats of the experiments. Motion of the hemocytes was tracked from live image movies using ImageJ. MARCM experiments were performed as described[49], with heat shock for 1h at 96–144h after egg laying.

Categories of injury induced responses. Initial studies piloting protocols and defining the responses were done on many animals. Subsequently we performed experiments for quantitative analysis of the injury response. After detailed observation, we devised scoring categories that described the wing nerve response up to 14 d. Any single wing displayed only a single biological response, and therefore allowed the unambiguous assigning of each wing to a single category. The location of the first neural cell bodies of the wing margin are an unambiguous anatomical landmark because these neurons are large and are associated with a campaniform sensillum (white asterisks in Fig. 3a, b). GFP loss to these neurons or GFP loss beyond these neurons comprised two clear and unambiguous classes: Local Loss, where GFP loss occurred between the injury site and these neuronal bodies; Broad Loss, where GFP loss extended beyond these neuronal bodies along the wing margin. GFP to Injury had GFP expression to the site of ablation, which was unambiguous because it was localized just below the first cell bodies of the costal vein and was associated with a pigment scar. GFP to Injury frequently showed a splayed projection pattern. Misrouting was distinct as GFP axons projecting into the costal vein; normally, there is never GFP between the L1 vein and the most distal (to the wing tip) neurons along the costal vein. We largely limited our studies to 14d, because at later time points, GFP loss occurred in unablated wings due to ageing (deterioration of the nervous system, damage, or physical usage of the wing). Upon expression of Bsk-DN, a new class never seen before was detected as GFP through the injury site. Nerve ablation with the snapback of the GFP nerve tract upon severing was seen in all of these wings. Each time point graphed represents the mean

response of 3 sets of animals, each set was typically comprised of 10 animals (typical range 10–16, maximum 23, a few cases had less than 10). The responses are presented as mean ± SD. Data were analyzed by ANOVA for significance, then Tukey's multiple comparison test (GraphPad Prism).

Dye injection. Live animals were injected with fluorescently labeled 3,000 MW Dextrans (Life Technologies, Grand Island, NY, Texas Red, lysine conjugated (cat. # D-3328) or neutrally charged (cat. # D-3329); results did not differ). Dextrans were dissolved in 1× PBS at 10 mg/ml, centrifuged 5 min to remove undissolved dye, aliquoted, stored at −20°C. Flies were anesthetized on CO_2 and mounted on agarose. A volume of 20–50 nl Dextrans were injected into the abdominal hemolymph with an Eppendorf FemtoJet and Femtotip needles (Eppendorf NA, Hauppauge, NY) (Supplementary Figure S1 shows exact position). Fluorescence in the wing vein hemolymph was observed in real time with epifluorescence microscopy on a Leica DM6000B compound microscope.

1. Benowitz, L. I., Goldberg, D. E. & Irwin, N. Inosine stimulates axon growth in vitro and in the adult CNS *Prog. Brain Res.* **137**, 389–399 (2002).
2. Chaudhry, N. & Filbin, M. T. *Myelin-associated inhibitory signaling and strategies to overcome inhibition. J. Cereb. Blood Flow Metab.* **27**, 1096–1107 (2007).
3. Filbin, M. T. How inflammation promotes regeneration. *Nat. Neurosci.* **9**, 715–717 (2006).
4. Fitch, M. T. & Silver, J. CNS injury, glial scars, and inflammation: Inhibitory extracellular matrices and regeneration failure. *Exp. Neurol.* **209**, 294–301 (2008).
5. Horn, K. P., Busch, S. A., Hawthorne, A. L., van Rooijen, N. & Silver, J. Another barrier to regeneration in the CNS: activated macrophages induce extensive retraction of dystrophic axons through direct physical interactions. *J. Neurosci.* **28**, 9330–9341 (2008).
6. Schwab, M. E. & Bartholdi, D. *Degeneration and regeneration of axons in the lesioned spinal cord. Physiol. Rev.* **76**, 319–370 (1996).
7. Fang, Y. & Bonini, N. M. Axon degeneration and regeneration: insights from *Drosophila* models of nerve injury. *Ann. Rev. Cell Dev. Biol.* **28**, 575–597 (2012).
8. Chen, L. & Chisholm, A. D. Axon regeneration mechanisms: insights from *C. elegans. Trends Cell Biol.* **21**, 577–584 (2011).
9. Coleman, M. P. & Freeman, M. R. Wallerian degeneration, wld(s), and nmnat. *Annu. Rev. Neurosci.* **33**, 245–267 (2010).
10. El Bejjani, R. & Hammarlund, M. Neural regeneration in *Caenorhabditis elegans. Annu. Rev. Genet.* **46**, 499–513 (2012).
11. Liu, K., Tedeschi, A., Park, K. K. & He, Z. Neuronal intrinsic mechanisms of axon regeneration. *Annu. Rev. Neurosci.* **34**, 131–152 (2011).
12. Sirbulescu, R. F. & Zupanc, G. K. Spinal cord repair in regeneration-competent vertebrates: adult teleost fish as a model system. *Brain Res. Rev.* **67**, 73–93 (2011).
13. Case, L. C. & Tessier-Lavigne, M. Regeneration of the adult central nervous system. *Curr. Biol.* **15**, R749–753 (2005).
14. Leyssen, M., Ayaz, D., Hebert, S. S., Reeve, S., De Strooper, B. & Hassan, B. A. Amyloid precursor protein promotes post-developmental neurite arborization in the Drosophila brain. *EMBO J.* **24**, 2944–2955 (2005).
15. Xiong, X., Wang, X., Ewanek, R., Bhat, P., Diantonio, A. & Collins, C. A. Protein turnover of the Wallenda/DLK kinase regulates a retrograde response to axonal injury. *J. Cell Biol.* **191**, 211–223 (2010).
16. Stone, M. C., Nguyen, M. M., Tao, J., Allender, D. L. & Rolls, M. M. Global up-regulation of microtubule dynamics and polarity reversal during regeneration of an axon from a dendrite. *Mol. Biol. Cell.* **21**, 767–777 (2010).
17. Kato, K., Forero, M. G., Fenton, J. C. & Hidalgo, A. The glial regenerative response to central nervous system injury is enabled by pros-notch and pros-NFkappaB feedback. *PLoS Biol.* **9**, e1001133 (2011).
18. Hoopfer, E. D., McLaughlin, T., Watts, R. J., Schuldiner, O., O'Leary, D. D. & Luo, L. Wlds protection distinguishes axon degeneration following injury from naturally occurring developmental pruning. *Neuron.* **50**, 883–895 (2006).
19. Fang, Y., Soares, L., Teng, X., Geary, M. & Bonini, N. M. A novel *Drosophila* model of nerve injury reveals an essential role of Nmnat in maintaining axonal integrity. *Curr. Biol.* **22**, 590–595 (2012).
20. MacDonald, J. M., Beach, M. G., Porpiglia, E., Sheehan, A. E., Watts, R. J. & Freeman, M. R. The *Drosophila* cell corpse engulfment receptor Draper mediates glial clearance of severed axons. *Neuron.* **50**, 869–881 (2006).
21. Hartenstein, V. & Posakony, J. W. Development of adult sensilla on the wing and notum of *Drosophila melanogaster. Development.* **107**, 389–405 (1989).
22. Murray, M. A., Schubiger, M. & Palka, J. Neuron differentiation and axon growth in the developing wing of *Drosophila melanogaster. Dev. Biol.* **104**, 259–273 (1984).
23. Fang, Y., Soares, L. & Bonini, N. M. Design and implementation of in vivo imaging of neural injury responses in the adult *Drosophila* wing. *Nat. Protoc.* **8**, 810–819 (2013).
24. Tuck, E. & Cavalli, V. Roles of membrane trafficking in nerve repair and regeneration. *Commun. Integr. Biol.* **3**, 209–214 (2010).
25. Song, Y., Ori-McKenney, K. M., Zheng, Y., Han, C., Jan, L. Y. & Jan, Y. N. Regeneration of *Drosophila* sensory neuron axons and dendrites is regulated by the Akt pathway involving Pten and microRNA bantam. *Genes Dev.* **26**, 1612–1625 (2012).
26. Zheng, Y. *et al.* Dynein is required for polarized dendritic transport and uniform microtubule orientation in axons. *Nat. Cell Biol.* **10**, 1172–1180 (2008).
27. Hatan, M., Shinder, V., Israeli, D., Schnorrer, F. & Volk, T. The *Drosophila* blood brain barrier is maintained by GPCR-dependent dynamic actin structures. *J. Cell Biol.* **192**, 307–319 (2011).
28. Riedl, J. *et al.* Lifeact: a versatile marker to visualize F-actin. *Nat. Methods.* **5**, 605–607 (2008).
29. Peri, F. Breaking ranks: how leukocytes react to developmental cues and tissue injury. *Curr. Opin. Genet. Dev.* **20**, 416–419 (2010).
30. Tepass, U., Fessler, L. I., Aziz, A. & Hartenstein, V. Embryonic origin of hemocytes and their relationship to cell death in *Drosophila. Development.* **120**, 1829–1837 (1994).
31. Wood, W. & Jacinto, A. *Drosophila melanogaster* embryonic haemocytes: masters of multitasking. *Nat. Rev. Mol. Cell Biol.* **8**, 542–551 (2007).
32. Osterwalder, T., Yoon, K. S., White, B. H. & Keshishian, H. A conditional tissue-specific transgene expression system using inducible GAL4. *Proc. Natl. Acad. Sci. U. S. A.* **98**, 12596–12601 (2001).
33. Byrne, A. B., Walradt, T., Gardner, K. E., Hubbert, A., Reinke, V. & Hammarlund, M. Insulin/IGF1 Signaling Inhibits Age-Dependent Axon Regeneration. *Neuron.* **81**, 561–573 (2014).
34. Bier, E. *Drosophila*, the golden bug, emerges as a tool for human genetics. *Nat. Rev. Genet.* **6**, 9–23 (2005).
35. Miller, B. R., Press, C., Daniels, R. W., Sasaki, Y., Milbrandt, J. & DiAntonio, A. *A dual leucine kinase-dependent axon self-destruction program promotes Wallerian degeneration. Nat. Neurosci.* **12**, 387–389 (2009).
36. Shin, J. E. *et al.* SCG10 is a JNK target in the axonal degeneration pathway. *Proc. Natl. Acad. Sci. U. S. A.* **109**, E3696–3705 (2012).
37. Ayaz, D. *et al.* Axonal injury and regeneration in the adult brain of *Drosophila. J. Neurosci.* **28**, 6010–6021 (2008).
38. Oliva, A. A., Jr., Atkins, C. M., Copenagle, L. & Banker, G. A. Activated c-Jun N-terminal kinase is required for axon formation. *J. Neurosci.* **26**, 9462–9470 (2006).
39. Quintanilla, R. A. *et al.* Thiazolidinediones promote axonal growth through the activation of the JNK pathway. *PLoS One.* **8**, e65140 (2013).
40. Qu, C. *et al.* c-Jun N-terminal kinase 1 (JNK1) is required for coordination of netrin signaling in axon guidance. *J. Biol. Chem.* **288**, 1883–1895 (2013).
41. Watkins, T. A. *et al.* DLK initiates a transcriptional program that couples apoptotic and regenerative responses to axonal injury. *Proc. Natl. Acad. Sci. U. S. A.* **110**, 4039–4044 (2013).
42. Nix, P., Hammarlund, M., Hauth, L., Lachnit, M., Jorgensen, E. M. & Bastiani, M. Axon Regeneration Genes Identified by RNAi Screening in *C. elegans. J. Neurosci.* **34**, 629–645 (2014).
43. Tank, E. M., Rodgers, K. E. & Kenyon, C. Spontaneous age-related neurite branching in *Caenorhabditis elegans. J. Neurosci.* **31**, 9279–9288 (2011).
44. Toth, M. L. *et al.* Neurite sprouting and synapse deterioration in the aging *Caenorhabditis elegans* nervous system. *J. Neurosci.* **32**, 8778–8790 (2012).
45. Edwards, S. L., Yu, S. C., Hoover, C. M., Phillips, B. C., Richmond, J. E. & Miller, K. G. An organelle gatekeeper function for *Caenorhabditis elegans* UNC-16 (JIP3) at the axon initial segment. *Genetics.* **194**, 143–161 (2013).
46. Pfeiffer, B. D. *et al.* Refinement of tools for targeted gene expression in *Drosophila. Genetics.* **186**, 735–755 (2010).
47. Shen, J., Curtis, C., Tavare, S. & Tower, J. A screen of apoptosis and senescence regulatory genes for life span effects when over-expressed in *Drosophila. Aging (Albany NY).* **1**, 191–211 (2009).
48. Byrne, A. B., Edwards, T. J. & Hammarlund, M. In vivo laser axotomy in *C. elegans. J. Vis. Exp.* **51**, e2707; *DOI: 10.3791/2707* (2011).
49. Lessing, D. & Bonini, N. M. Polyglutamine genes interact to modulate the severity and progression of neurodegeneration in *Drosophila. PLoS Biol.* **6**, e29; *DOI:10.1371/journal.pbio.0060029* (2008).

Acknowledgments

Author contributions

The research was designed by L.S. and N.B.; experiments were performed by L.S. and M.P.; L.S. and N.B. wrote the manuscript with input from M.P.

Additional information

Supplementary information accompanies this paper at http://www.nature.com/scientificreports